AIAA JOURNAL
Vol. 38, No. 4, April 2000

Numerical Study of Wake Vortex Decay and Descent in Homogeneous Atmospheric Turbulence

Jongil Han,* Yuh-Lang Lin,† and S. Pal Arya‡
North Carolina State University, Raleigh, North Carolina 27695-8208
and
Fred H. Proctor§
NASA Langley Research Center, Hampton, Virginia 23681-2199

Numerical simulations are performed to isolate the effect of ambient turbulence on the wake vortex decay rate within a neutrally stratified atmosphere. Simulations are conducted for a range of turbulence intensities by injecting wake vortex pairs into an approximately homogeneous and isotropic turbulence field. Consistent with field observations, the decay rate of the vortex circulation increases clearly with increasing levels of ambient turbulence. Based on the results from the numerical simulations, simple decay models for the vortex pair are proposed as functions of nondimensional ambient turbulence intensity, nondimensional radial distance, and nondimensional time. For strong atmospheric turbulence, the model predictions are in reasonable agreement with the observational data. For weak turbulence with stable stratification, the model, based on turbulence dissipation alone, underestimates circulation decay with consistent overestimation of vortex descent, unless stratification effects are included.

Nomenclature

B	= aircraft wingspan
b_0	= initial vortex separation distance, $\pi B/4$
c_s	= coefficient for filter width in the subgrid model, 0.16
c_1, c_2	= model coefficients for vortex decay, 0.13 and 0.08, respectively
D	= rate of velocity deformation
d_1, d_2	= model coefficients for vortex descent, 0.84 and 0.71, respectively
$F_{\beta\beta}$	= one-dimensional spectra
H	= nondimensional vortex descent distance, h/b_0
h	= vortex descent distance from initial vortex elevation
I_1, I_2	= isotropy parameters, $[\langle u^2\rangle/\langle w^2\rangle]^{1/2}$ and $[\langle v^2\rangle/\langle w^2\rangle]^{1/2}$, respectively
K	= subgrid eddy viscosity
L_x, L_y, L_z	= domain sizes in x, y, and z directions, respectively
L_{33}	= integral length scale of turbulence in z direction
N	= Brunt–Väisälä frequency
q	= turbulent velocity scale, $(\overline{u^2} + \overline{v^2} + \overline{w^2})^{1/2}$
R	= nondimensional radial distance from vortex center
Re	= circulation Reynolds number, Γ/ν
Ri_R	= rotational Richardson number
Ri_S	= Richardson number due to stratification, N^2/D^2
r	= radial distance from vortex center
r_c	= initial core radius defined as radial distance of peak tangential velocity
T	= nondimensional time, tV_0/b_0
t	= time
t_e	= large-eddy turnover time, $L_{33}/\langle w^2\rangle^{1/2}$
u, v, w	= velocities in x, y, and z directions, respectively
u_n'	= fluctuation of velocity normal to the surface
V	= tangential velocity
V_a	= airspeed of generating aircraft
V_0	= initial vortex induction speed, $\Gamma_\infty/(2\pi b_0)$
W	= aircraft weight
x, y, z	= axial, lateral, and vertical space coordinate relative to initial vortex system
α	= coefficient for Ri_S, 3.0
β	= coefficient for Ri_R, 1.5
Γ	= vortex circulation
Γ_0	= initial circulation
Γ_∞	= initial circulation at $r \gg r_c$, $4W/(\pi B\rho V_a)$
Δ	= filter width in the subgrid model, $(2\Delta x\, 2\Delta y\, 2\Delta z)^{1/3}$
Δx, Δy, Δz	= grid sizes in x, y, and z directions, respectively
ϵ	= turbulent kinetic energy dissipation rate
ζ	= axial vorticity
ζ'	= fluctuation of axial vorticity
η	= nondimensional ambient turbulence intensity, $(\epsilon b_0)^{1/3}/V_0$
$\Theta(z)$	= ambient potential temperature profile
κ	= wave number
Λ	= integral length scale of turbulence
ν	= kinematic viscosity
ν_e	= effective turbulent eddy viscosity
ρ	= air density
Ω	= three-dimensional vorticity

Received 16 November 1998; revision received 18 June 1999; accepted for publication 3 September 1999. This material is declared a work of the U.S. Government and is not subject to copyright protection in the United States.

*Research Scientist, Department of Marine, Earth and Atmospheric Sciences. Member AIAA.
†Professor, Department of Marine, Earth and Atmospheric Sciences; yl_lin@ncsu.edu. Member AIAA.
‡Professor, Department of Marine, Earth and Atmospheric Sciences.
§Research Scientist, Airborne Systems Competency. Member AIAA.

I. Introduction

FOR the purpose of increasing airport capacity, a system is being developed under NASA's Terminal Area Productivity Program that will control aircraft spacing within the narrow approach corridors of airports. The system, called the Aircraft Vortex Spacing System,[1,2] will determine safe operating spacing between arriving and departing aircraft as based on the observed or predicted weather conditions. This system will provide a safe reduction in separation of aircraft compared to the now-existing flight rules, which are based on aircraft weight categories. To develop this system, research is being focused on understanding how aircraft wake vortices interact with the atmosphere. Previous studies indicate that transport and decay of wake vortices are strongly affected by ambient atmospheric parameters such as wind shear, stratification, and turbulence, as well as by proximity of aircraft to the ground.[3] In this study we focus on the effects of three-dimensional ambient atmospheric turbulence on vortex decay and descent using a validated large-eddy simulation (LES) model.

The mechanisms and causes for the decay of the wake vortices have been somewhat controversial.[4] Some researchers believe that vortices generally do not decay until three-dimensional instabilities such as Crow instability[5] lead to their sudden destruction.[6] However, this view is held in spite of the overwhelming observational evidence that vortices do decay at different rates depending on the ambient meteorological conditions,[3] and atmospheric turbulence plays a key role.[7,8] Recent analyses of field observation data by Sarpkaya[9] clearly show that vortex circulation decays much faster in the presence of strong turbulence than in weak turbulence. Using a second-order turbulence closure model, Bilanin et al.[10] show that the rate of decay of a vortex pair increases with increasing dissipation rate of background turbulence. From three-dimensional LES of wake vortices in a realistic atmospheric boundary layer, Corjon and Darracq[11] reveal that the vortices decay with time in a turbulent environment. Our analyses of LES data[3,12,13] also reveal that three-dimensional atmospheric turbulence enhances vortex decay. On the other hand, the descent speed of a vortex pair due to mutual induction decreases with decreasing circulation as long as the separation distance of a vortex pair remains constant. From the data obtained in their water tank experiments, Sarpkaya and Daly[14] find that the descent speed of vortices decreases with increasing dissipation rate of the ambient turbulence. This, in turn, implies that stronger turbulence yields larger reduction in circulation. Stable stratification $[\partial\Theta(z)/\partial z > 0$, where $\Theta(z)$ is the ambient potential temperature profile] can also hasten vortex decay through baroclinic generation of countersign vorticity along the vortex oval's periphery.[3,15,16] Because most of field observation data are subjected to the influence of both turbulence and stratification, it is difficult to distinguish each of their effects on circulation decay and vortex descent. In the present study, we consider only a neutrally stratified atmosphere, that is, $\partial\Theta(z)/\partial z = 0$, to isolate the effects of atmospheric turbulence on vortex decay. Our other ongoing investigations of wake vortex decay in nonneutral environments will be reported in a future paper.

The acceleration of vortex decay by ambient turbulence has been an important factor in several wake-vortex prediction models.[7,8] Donaldson and Bilanin[7] proposed a formula describing the relation between atmospheric turbulence and decay of vortex circulation:

$$\frac{\mathrm{d}\Gamma}{\mathrm{d}t} = -0.82\frac{q\Gamma}{b_0} \tag{1}$$

Greene[8] incorporated Eq. (1) into his analytic model to account for the contribution of atmospheric turbulence effects on wake vortex motion and decay. Equation (1) implies that vortex circulation decays exponentially and depends only on ambient turbulence, represented by q, which is related to the turbulence kinetic energy (TKE $= q^2/2$). The TKE (or q) is primarily determined by the large energy-containing eddies. According to Eq. (1), large-scale eddies are involved in the decay of vortex circulation. Although large energy-containing eddies can lead to a large deformation and transport of vortices as well as to the development of the large-scale Crow instability,[3,17–19] it is the small-scale (order of b_0 and less) turbulent eddies that are directly associated with the decay of vortex circulation. These small scales of turbulent eddies are likely to be more homogeneous and isotropic and most often lie within the Kolmogorov inertial subrange that is characterized only by turbulent kinetic energy dissipation rate (ϵ) (Ref. 20). Therefore, ϵ rather than q is a more appropriate turbulence parameter for controlling the vortex decay.

In fact, ϵ has been commonly used in the literature[14,18,19,21,22] as an appropriate parameter to represent the effects of ambient turbulence on the lifespan of wake vortices. The strength of turbulence is often represented by the nondimensional turbulence intensity η defined as

$$\eta = (\epsilon b_0)^{\frac{1}{3}}/V_0 \tag{2}$$

where

$$V_0 = \Gamma_\infty/2\pi b_0 \tag{3}$$

Note that η is the ratio of the characteristic turbulent velocity scale at the scale of the vortex separation distance $(\epsilon b_0)^{1/3}$ to the initial descent speed of the vortex pair by mutual induction, V_0.

Our studies are focused on the far-field, postrollup stage of the vortex pair, in which each vortex possesses a well-developed structure. For later discussion, we define nondimensional parameters for time t, descent distance of the vortices, h, and radial distance r as

$$T = V_0 t/b_0, \qquad H = h/b_0, \qquad R = r/b_0 \tag{4}$$

In Sec. II, we describe the LES model and the modifications required for the initial conditions. In Sec. III, we present the results from systematic numerical experiments in terms of nondimensional turbulence intensity and also propose new vortex models for vortex decay and descent, based on the LES results. In Sec. IV, we apply the proposed models to available observation data. Finally, in Sec. V, we summarize our results and draw some conclusions.

II. Model and Initial Conditions

The model formulation and initial conditions must be chosen with great care when applied to the numerical simulation of wake vortices. Atmospheric wake vortices are three-dimensional, have very high Reynolds numbers, and are embedded within turbulent flow.[9] Hence, laminar simulations, especially at low Reynolds numbers, are inappropriate for studies of wake vortex decay. The numerical approximations assumed for wake vortex simulations should be stable, nondiffusive, and accurate, yet computationally efficient.

A. Model

The numerical model used in the present study is a three-dimensional, nonlinear, compressible LES model, called the terminal area simulation system[23] (TASS), which has been adopted for simulation of interaction of wake vortices with the atmosphere.[24–26] The TASS model contains 12 prognostic equations: 3 for momentum, 1 each for pressure deviation and potential temperature, 6 coupled equations for continuity of water substance (water vapor, cloud droplet, cloud ice crystals, rain, snow, and hail), and 1 for a massless tracer. In the present study, we use only four equations for momentum and pressure deviation because we assume statically neutral, dry atmosphere.

The TASS model uses the time-splitting integration procedure (small time step for acoustically active terms and large time step for advection and diffusion[27]) that results in a substantial savings in computing time. Local time derivatives (both small and large time steps) are approximated by the second-order Adams–Bashforth method. Space derivatives are approximated by central differences in quadratic-conservative form, which are fourth-order for advective derivatives and second-order for remaining derivatives. Details of the numerical formulation can be found by Proctor.[23,24] The numerical schemes used in TASS produce accurate and stable results and have been shown to have almost no numerical dissipation.[28] In Ref. 3 for a two-dimensional laminar simulation result with a very small constant viscosity ($Re \equiv \Gamma/\nu \sim 10^6$), it was shown that the tangential velocity does not change with time from the initial profile, indicating that TASS is essentially free of numerical dissipation.

Turbulence is strongly affected by the rotation of the swirling vortex flow. According to Rayleigh's well-known stability criterion,[29] perturbations are suppressed in an axisymmetric vortex if the circulation is increasing with radial distance, but perturbations would become unstable if the circulation is decreasing with radial distance. Because the circulation increases rapidly with radial distance in the vortex core region, any preexisting turbulence is suppressed there, and the vortex core (defined as the radius of maximum tangential velocity) expands very little with time.[9,16] In the present numerical model, an expression for the subgrid eddy viscosity that accounts for the flow rotation effects is used to avoid unrealistic core growth as described subsequently.

For subgrid turbulence, TASS currently uses a conventional Smagorinsky model[30] with modifications for stratification effects as

$$K = (c_s\Delta)^2|D|(1 - \alpha Ri_S)^{0.5} \tag{5}$$

Note that Ri_S is included here, although it has no contribution because stratification is not considered in the present study.

A simple modification of the subgrid eddy viscosity for the effects of flow rotation has been developed in Ref. 31 following the suggestion by Rubinstein and Zhou.[32] In this formulation, rotation

acts to suppress subgrid turbulence, in a way that is analogous to the effects from stratification, and is given as

$$K = (c_s\Delta)^2|D|(1 - \alpha Ri_S - \beta Ri_R)^{0.5} \quad (6)$$

Here rotational Richardson number Ri_R is defined as

$$Ri_R = \Omega^2/D^2 + |\Omega|/|D| \quad (7)$$

Equations (6) and (7) indicate that the eddy viscosity K can be effectively reduced within the core of vortices due to large $|\Omega|/|D|$. Because the preceding formula cannot discriminate between shear flow and flow with coherent rotation, a discriminator function is applied that turns the formula off (defaulting to the original Smagorinsky model) in the absence of coherent rotation. Details of this formula may also be found in Ref. 31. The coefficient for β is chosen empirically, with a value of 1.5. This value for β was chosen large enough to suppress mixing across the vortex core and is assumed to be universal for all situations. This formulation, with $\beta = 1.5$, was also applied to a three-dimensional LES simulation of homogeneous turbulence with no detectable corruption of the energy spectrum. One of the beneficial consequences of the formulation is to prevent the vortex core from growing with time, as verified from field measurements.[9] In experiments with the unmodified Smagorinsky model [Eq. (5)], the vortex core was found to unrealistically expand with time.[33]

Periodic boundary conditions are imposed at all domain boundaries. The domain size used in our simulations is $(L_x, L_y, L_z) = (2.5b_0, 5b_0, 5b_0) = (80\Delta x, 160\Delta y, 160\Delta z)$, where $b_0 = 32$ m, the grid size $\Delta x = \Delta y = \Delta z = 1$ m, x, y, and z correspond to the axial, lateral, and vertical directions of the vortex system, and the corresponding velocity components are u, v, and w, respectively. The smaller domain size in the axial direction, $2.5b_0$, which can save much computing time, suppresses the development of Crow instability of which the theoretical maximum wavelength is about $8.6b_0$ (Ref. 5), and thus, statistically homogeneous decay behavior is anticipated along the axial direction. The domain size of $5b_0$ in the lateral and vertical directions is sufficiently large to minimize boundary influences. Comparison with a test case assuming a larger domain width showed little difference, indicating that $5b_0$ width was sufficiently large for this experiment. Because of our limited computing resources and to allow the core to be resolved, the initial core size ($r_c = 4$ m) is somewhat larger than the typical value observed behind aircraft (less than about 5% of the wingspan[24]). Obviously, with the importation of a fully periodic condition, any effect from the ground is omitted from these simulations; thus, the results are applicable to the free atmosphere only.

B. Initial Conditions

Because we want to study the effect of ambient turbulence on the vortex decay and descent within the free atmosphere, it is of crucial importance to obtain an initially homogeneous and isotropic turbulence field. Toward this purpose, the initial turbulence field is allowed to develop under an artificial external forcing at low wave numbers.[34] Because the TASS code uses a finite difference numerical scheme, the forcing is achieved by performing first a three-dimensional fast Fourier transform (FFT) at every large time step and then adding a constant amplitude to all of the modes with integer wave numbers whose magnitude is less than 3.0, and performing finally an inverse FFT back to the physical space. The wave number in the axial direction is normalized so that the axial wavelength has the same magnitude as that of the corresponding waves in lateral or vertical direction. Because of viscous dissipation, the simulation can reach a statistically steady state in the sense that the mean turbulence kinetic energy oscillates in time around a constant value.

Figure 1 shows the vertical velocity field and its one-dimensional longitudinal and transverse spectrum with $-\frac{5}{3}$ slope of Kolmogorov's spectrum when the turbulent flowfield reaches a statistically steady state. The calculated integral length scale is $L_{33} \approx 11.4$ m and the large-eddy turnover time, defined as $t_e = L_{33}/\langle w^2\rangle^{1/2}$, is estimated to be about 51.6 s. Here subscript 3 denotes the vertical direction and $\langle\ \rangle$ represents the domain average value. The isotropy parameter I, defined as $I_1 = [\langle u^2\rangle/\langle w^2\rangle]^{1/2}$

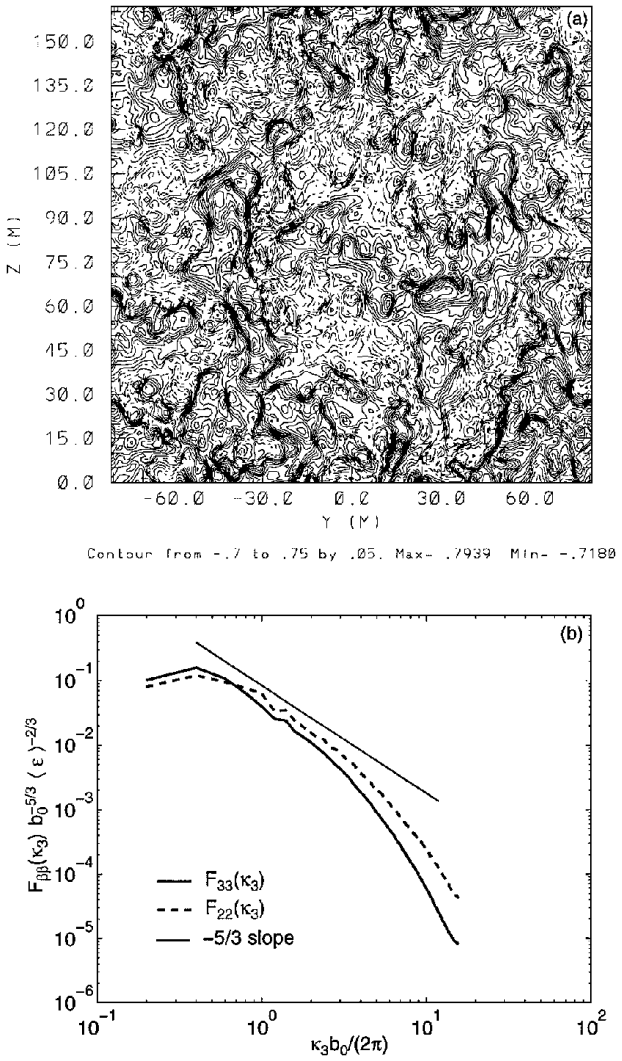

Fig. 1 Steady-state turbulence before vortex injection: a) vertical velocity field and b) its one-dimensional energy spectrum.

or $I_2 = [\langle v^2\rangle/\langle w^2\rangle]^{1/2}$, fluctuates only a few percent around its expected value of one for isotropic turbulence. Therefore, our simulated turbulence is close to statistical isotropy. The TKE dissipation rate ϵ is estimated by fitting Kolmogorov's theoretical spectrum in the inertial subrange to the simulated spectra in Fig. 1.

The initial vortex system is representative of the postrollup, wake-vortex velocity field. A vortex model recently developed by Proctor[3] is adopted in our experiments. This model is empirical because it is based on field observations of several wake vortices measured early in their evolution. Its tangential velocity V is represented as

$$V(r) = (\Gamma_\infty/2\pi r)\left\{1 - \exp\left[-10(r/B)^{0.75}\right]\right\} \quad (8)$$

Note that the velocity field in Eq. (8) depends on the wingspan B instead of the core radius r_c, which is not easy to accurately measure in field studies. Equation (8) is applicable only at $r > r_c$. For $r < r_c$, the model is matched with the Lamb model,[35] that is,

$$V(r) = (\Gamma_\infty/2\pi r)1.4\left\{1 - \exp\left[-10(r_c/B)^{0.75}\right]\right\} \times \left\{1 - \exp\left[-1.2527\,(r/r_c)^2\right]\right\} \quad (9)$$

The values assumed for initial vortex separation and circulation are derived from aircraft weight W, wingspan B, air density ρ, and airspeed V_a according to the conventional assumption of an elliptically loaded wing, that is,

$$b_0 = \pi B/4, \qquad \Gamma_\infty = 4W/\pi B\rho V_a$$

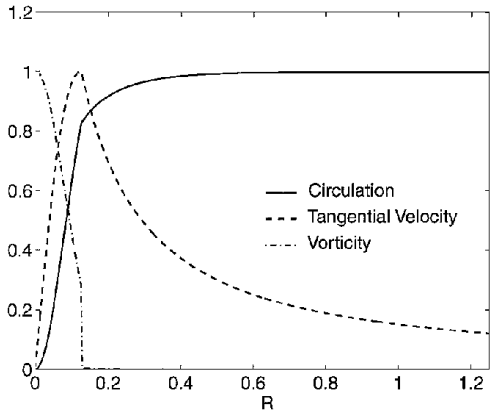

Fig. 2 Initial circulation, tangential velocity, and vorticity for each vortex normalized by their maximum values.

Normalized circulation, tangential velocity, and vorticity from the preceding model are shown in Fig. 2 as functions of the normalized radial distance $R = r/b_0$, assuming $r_c/b_0 = 0.125$.

A two-dimensional counter-rotating vortex pair following Eqs. (8) and (9) is initialized uniformly along the axial direction at the time when the ambient turbulence reaches a steady state after integration. To keep the vortices in the middle of the domain, the grid is allowed to translate downward at the speed of $0.9V_0$. Different values of nondimensional ambient turbulence strength η are obtained by varying the initial circulation Γ_∞ rather than by varying the initial turbulence field, that is, by varying ϵ, to save computing time. Simulations are conducted with dimensional quantities, although the results are presented in nondimensional forms to make them more generally applicable and independent of individual dimensional variables. Assuming that $\Gamma_\infty = 400\ \mathrm{m^2\ s^{-1}}$ and $b_0 = 40$ m, which are appropriate for large jet aircraft such as the DC-10, the range of values of η in the lower atmosphere is estimated to be 0.01–0.5, with the maximum value occurring during early afternoon convective conditions and the minimum value during very stable conditions after midnight.[3] Simulations are conducted for six values of η, which are within the given range. These cases are divided into three turbulence strength groups: $\eta = 0.0302$ and 0.0702 for weak turbulence, $\eta = 0.1006$ and 0.1509 for moderate turbulence, and $\eta = 0.3018$ and 0.5031 for strong turbulence. Generally, weak may represent the strength of typical boundary-layer turbulence during stable nighttime conditions and strong may represent typical strength during sunny daytime convective conditions. The simulated turbulence strengths represent a wide range of typical atmospheric conditions and aircraft sizes (note that η also depends on aircraft wingspan and the far-field circulation of its vortices). To isolate the effect of atmospheric turbulence on vortex decay from that of thermal stratification, all simulations assume neutral stratification.

III. Numerical Results

Simulation results for six values of η are presented. External forcing for maintaining ambient turbulence strength is deactivated to save computing time when the initial vortices are injected, but the difference in the results for maintaining or deactivating the forcing has been found to be negligible (not shown). This confirms the arguments by Corjon et al.[36] that the timescale of the ambient turbulence compared to that of the vortex is sufficiently large to obtain the main characteristics of the effects of ambient turbulence on the wake vortices.

During simulations, the vortices descend smoothly without any development of large-scale instabilities. As mentioned earlier, the Crow instability cannot occur in these simulations due to the small domain size in the axial direction.

The circulation at any radial distance r can be easily determined from the area integral of the axial vorticity ζ over a region defined by the radial distance, that is,

$$\Gamma_r = \int\int \zeta \, \mathrm{d}A \tag{10}$$

Table 1 Standard deviation of the circulation σ_Γ (%) relative to its mean value at the end of simulation time

η	T	σ_Γ at $3r_c$	σ_Γ at $4r_c$	σ_Γ at $5r_c$
0.0302	7	2.8	2.0	2.1
0.0702	6	3.8	4.1	4.3
0.1006	6	3.5	4.5	4.6
0.1509	6	6.6	9.0	9.9
0.3018	3	10.1	9.6	8.5
0.5031	3	31.4	28.2	23.1

Obtained at a fixed radial distance are a total of 160 circulation values for a pair of vortices in 80 y–z planes from which we have calculated averages and standard deviations. As shown in Table 1, the circulation fluctuations due to ambient turbulence increase with increasing turbulence level. The standard deviations appear to be small for most of turbulence levels (less than 10%) at least at the end of the simulation time, except for the strongest turbulence strength of $\eta = 0.5031$ for which the values are more than 20%. In the following, we consider only the average of circulations to deduce an appropriate model for vortex decay and descent.

A. Circulation Decay

Figure 3 shows the decay of circulation with time for varying radial distances, as well as varying ambient turbulence levels. As shown in Fig. 3, the decay rate of circulation increases clearly with increasing ambient turbulence level and appears to decrease with increasing radial distance, which is consistent with field observations.[9]

To investigate the vortex decay behavior in more detail for varying radial distances, the circulation evolution with a best-fitted function for each radial distance is plotted in Fig. 4 for relatively weak turbulence ($\eta = 0.0702$), in Fig. 5 for relatively moderate turbulence ($\eta = 0.1509$), and in Fig. 6 for strong turbulence ($\eta = 0.5031$). As evidenced in Figs. 4–6, the decay of the circulation appears to follow a Gaussian function e^{-aT^2} for weak and moderate turbulence (model G), whereas for strong turbulence, it appears to follow an exponential function e^{-bT} at smaller radial distances (model E) but a Gaussian function at larger radial distances, where a and b are functions of η and radial distance. Although only partly shown in Figs. 4–6, the circulation at radial distances larger than $0.6b_0$ appears to follow the Gaussian decay for all levels of turbulence. An exponential decay formula [Eq. (1)] was first proposed by Donaldson and Bilanin,[7] with q rather than ϵ as the turbulence parameter controlling the vortex decay. The Gaussian decay implies slower decay than the exponential decay during early evolution of the vortices. Based on our described LES results, two types of models (models E and G) are proposed for vortex decay and their formulations are given in the Appendix.

From the Appendix, Eqs. (A13) and (A17) can be rewritten in the nondimensional forms for model E as

$$\left.\frac{\mathrm{d}\Gamma}{\mathrm{d}T}\right|_{\text{turbulence}} = -c_1 \frac{\eta}{R^2}\Gamma \tag{11}$$

and for model G as

$$\left.\frac{\mathrm{d}\Gamma}{\mathrm{d}T}\right|_{\text{turbulence}} = -2c_2 \frac{\eta^2 T}{R^2}\Gamma \tag{12}$$

where c_1 and c_2 are empirical constants. Further integrations of Eqs. (11) and (12) with respect to nondimensional time (assuming ambient turbulence is only the process affecting vortex decay) yields for model E

$$\Gamma = \Gamma_0 \exp\left[-\left(c_1 \eta / R^2\right) T\right] \tag{13}$$

and yields for model G

$$\Gamma = \Gamma_0 \exp\left[-\left(c_2 \eta^2 / R^2\right) T^2\right] \tag{14}$$

(It is assumed that η does not change with time.)

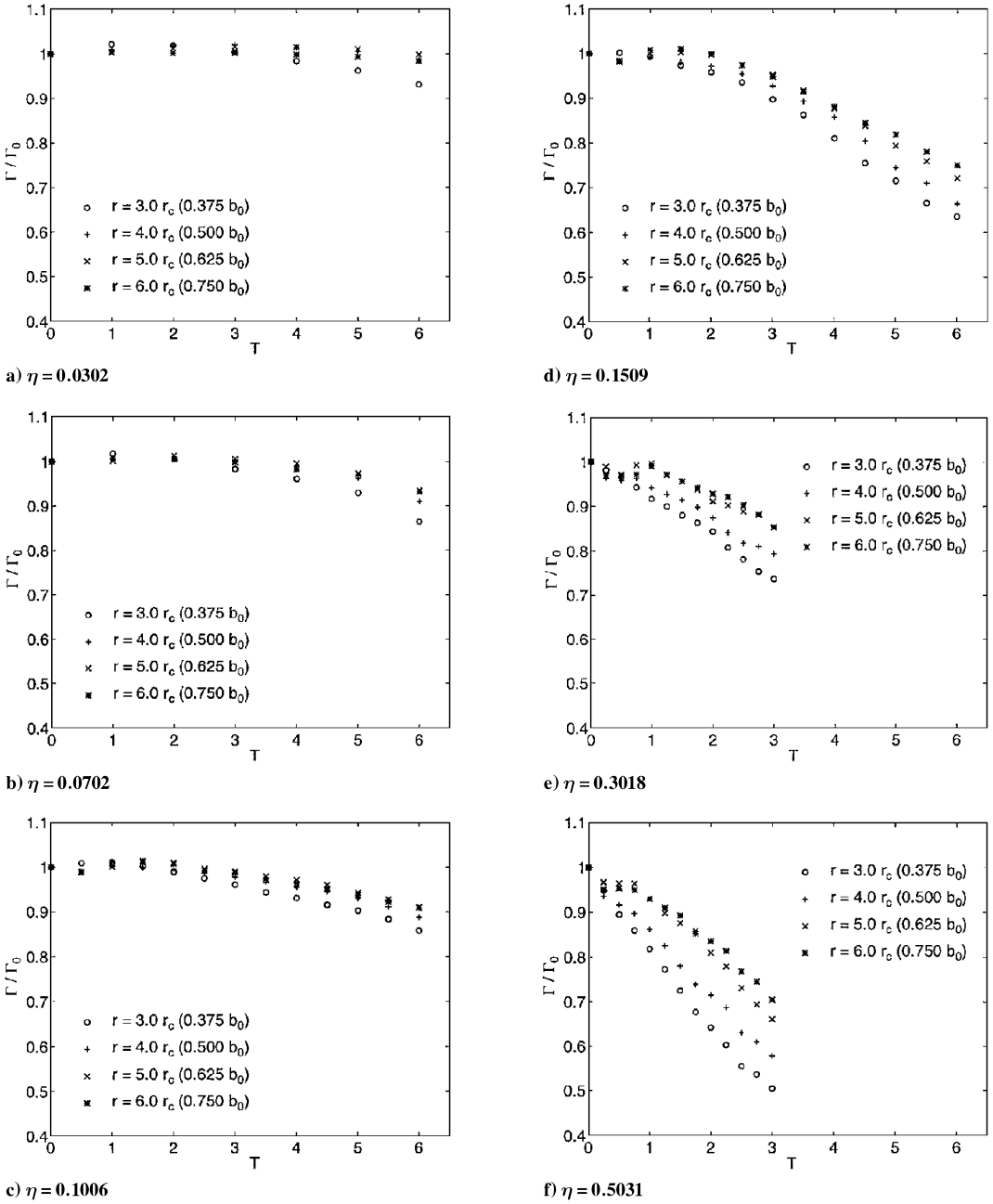

Fig. 3 Decay of circulation with time for varying radial distances and ambient turbulence strengths.

In a transition range from moderate to strong ambient turbulence levels, which is about $\eta = 0.25-0.30$ in the present study, the decay behavior of the vortices appears to be more complicated due to the dependency of the model types on radial distances. For example, in this range of η, the vortex decay follows model E in a smaller range of radial distances, whereas it follows model G in a larger range of radial distances: The range of radial distances for the applicability of model E increases with increasing ambient turbulence level but may not be a linear function of η. For a practical purpose, nevertheless, we propose a simple model in the transition range that is a composite of models E and G weighted linearly with varying η ($0.25 < \eta < 0.30$) as

$$\Gamma = [(\eta - \eta_1)/\Delta\eta]\Gamma_E + [(\eta_2 - \eta)/\Delta\eta]\Gamma_G \tag{15}$$

where η_1 and η_2 are lower and upper limits of the transition range, $\Delta\eta = \eta_2 - \eta_1$, and Γ_E and Γ_G are the circulations given by Eqs. (13) and (14), respectively.

Previous investigators have quantified the strength of a vortex in terms of a parameter called average circulation that is defined as[24,37]

$$\bar{\Gamma}_{r_1,r_2} = \frac{1}{r_2 - r_1}\int_{r_1}^{r_2} \Gamma \, dr \tag{16}$$

where r_1 and r_2 are the radial distances of the averaging interval. This parameter is desirable because it relates to the rolling moment of an encountering aircraft and provides a more stable measurement than the local circulation.[24,37] In particular, the average circulation within 15 m from the vortex center has been considered to be closely related to the hazard.[38,39] In the present study, we consider the average circulation from $R = 0.4$ to 0.6 because the circulation decay in this range of radial distances is not very sensitive to grid resolution. The average circulation in the following represents the circulation averaged over the range of $R = 0.4-0.6$ according to Eq. (16) unless stated otherwise.

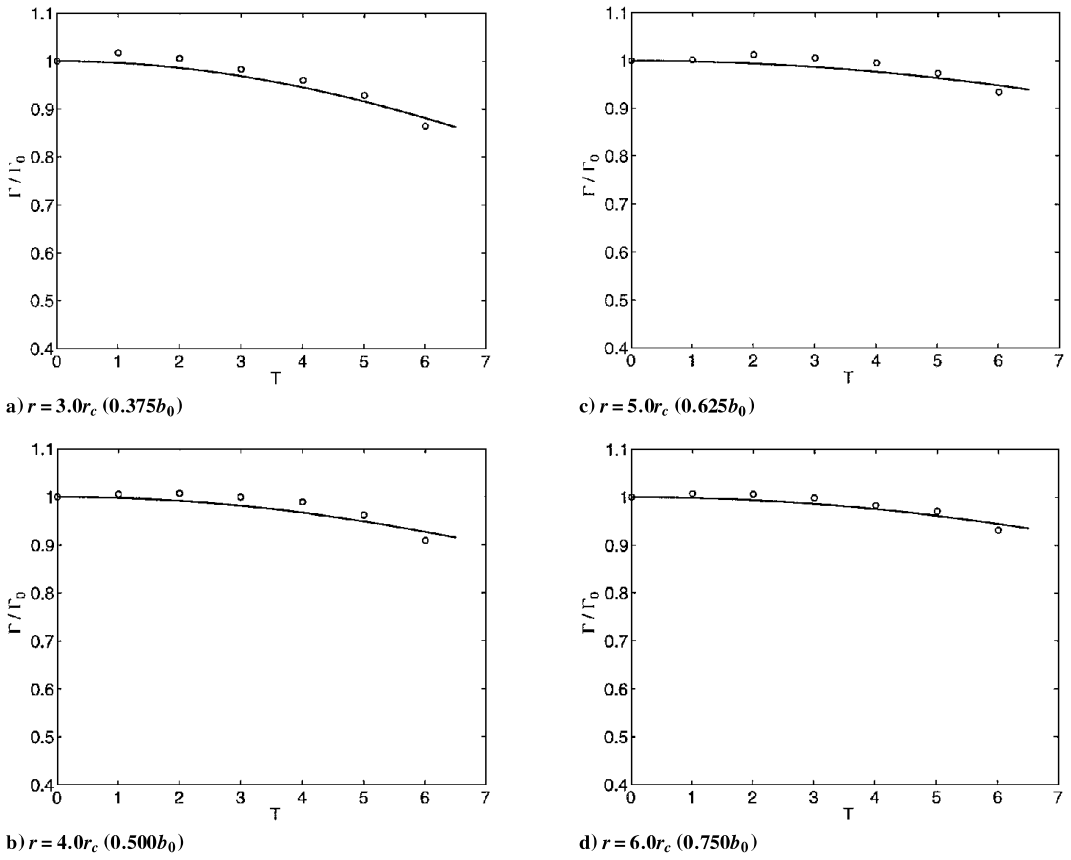

Fig. 4 Circulation decay and best-fitted functions at four different radial distances for $\eta = 0.0702$ (weak turbulence): solid line indicates e^{-aT^2}, where a is a function of η and R.

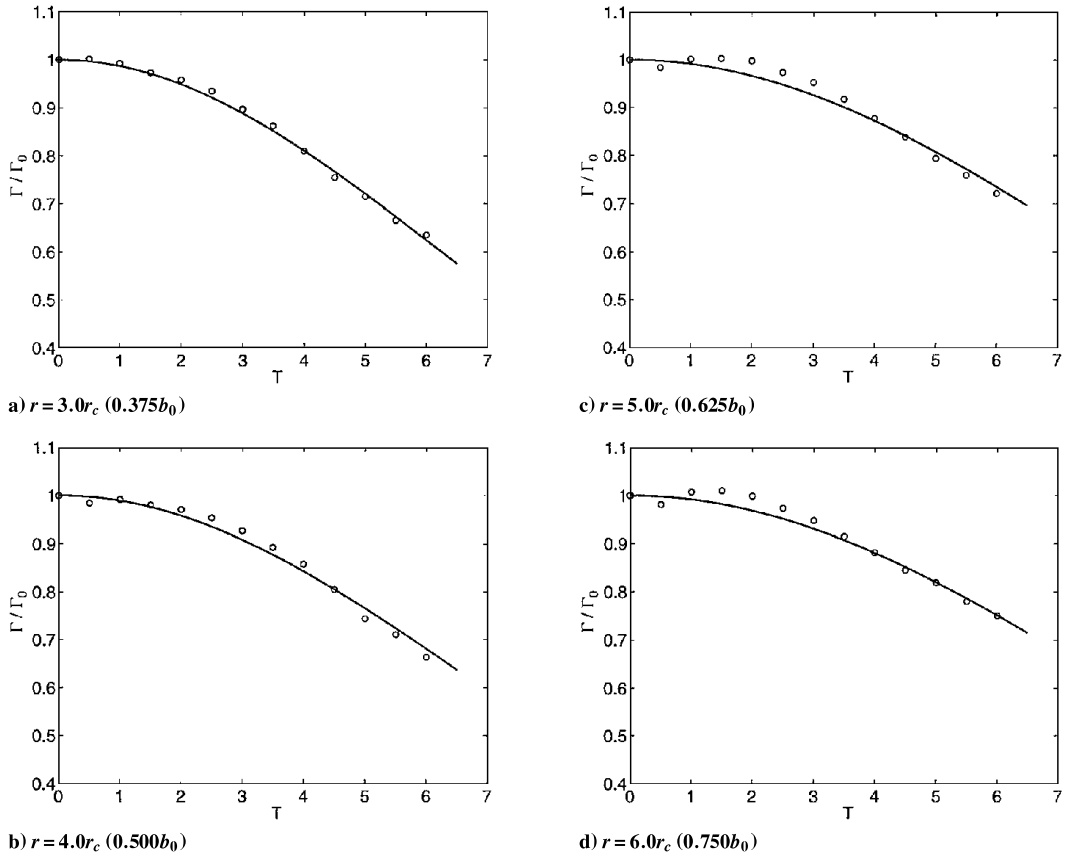

Fig. 5 Same as Fig. 4 but for $\eta = 0.1509$ (moderate turbulence).

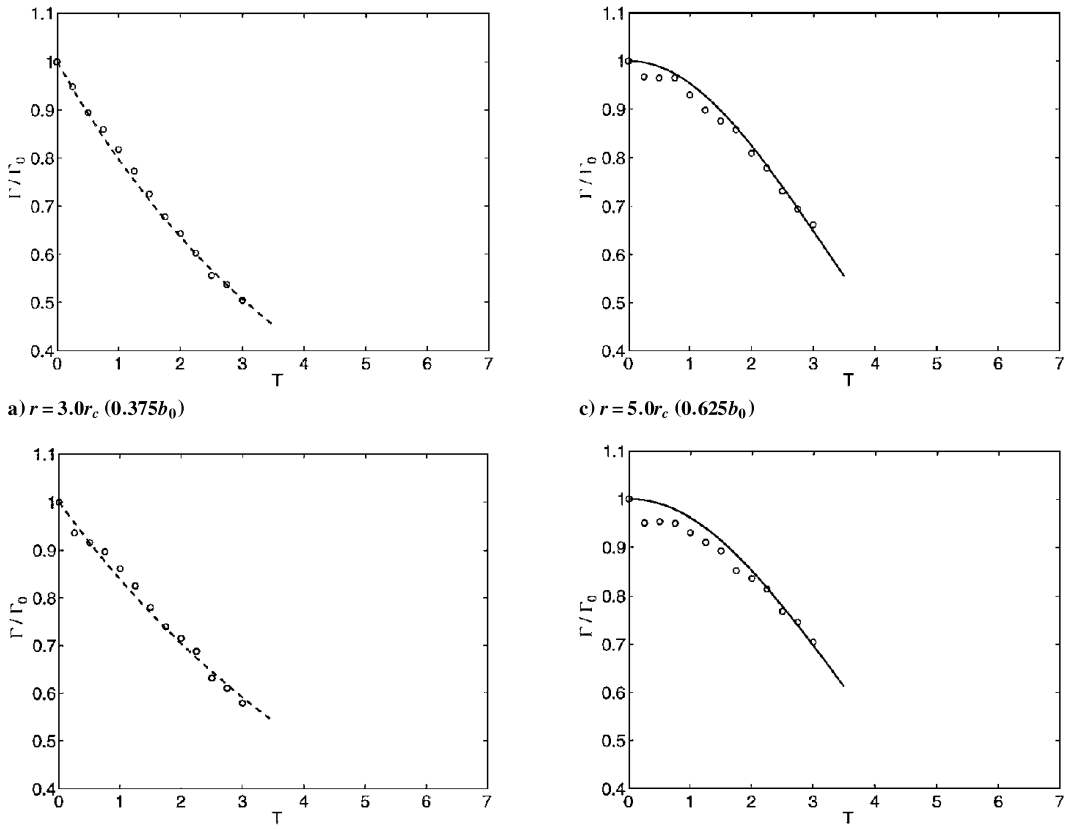

Fig. 6 Same as Fig. 4 but for $\eta = 0.5031$ (strong turbulence): dashed line indicates e^{-bT}, where b is a function of η and R.

As can be seen from Fig. 7, the average circulations from the model predictions, that is, Eqs. (13) and (14), agree much better with the LES data than the local circulations, showing a Gaussian decay for weak and moderate turbulence but an exponential decay for strong turbulence. The model coefficients represented in Fig. 8 are obtained from the average circulation and do not appear to fluctuate significantly with varying η in spite of the highly irregular nature of turbulence. To obtain a representative model coefficient, more experiments have been performed for different η values and for different initial turbulence fields. The values of coefficients (Fig. 8) fluctuate with varying η within the ranges of $c_1 = 0.06-0.09$ and $c_2 = 0.08-0.20$, respectively. The mean values of the coefficients, which can be considered as more representative, are $c_1 = 0.08$ for model E and $c_2 = 0.13$ for model G, respectively.

Using the given mean values of the coefficients, our model predictions at $R = 0.5$ for various ambient turbulence levels are plotted in Fig. 9. Crow instability is a well-known phenomenon in which the vortex pair undergoes a symmetric and sinusoidal instability that grows exponentially and finally results in a linking (merging) into a series of crude vortex rings. The vortex lifespans shown in Fig. 9, defined as the time at which linking of a vortex pair occurs as a result of the Crow instability, are obtained from a model recently developed by Sarpkaya,[9] where the linking time is given as only a function of η. This model is a revised one from the original Crow and Bate's[21] model and has been shown to agree well with data from water tank experiments[14] and LES predictions.[19] Figure 9 indicates that, until a linking of the vortices occurs, the circulation is reduced by only about 2% of its initial value for weak ambient turbulence ($\eta = 0.03$), whereas it may be reduced by as much as 20% for strong ambient turbulence ($\eta = 0.50$).

B. Vortex Descent

The descent of an ideal vortex pair, where vorticity is concentrated in two parallel lines, will follow the relation of $H = T$ in an inviscid fluid. In the numerical simulation, however, descent rate of a pair of the vortices can deviate from $H/T = 1$ due to the influence of image vortices implicit on the assumption of periodic boundary conditions and the use of a vortex model different from ideal line vortices. From a two-dimensional laminar simulation with the same domain size as the cross plane size of the preceding three-dimensional simulation and with a very small constant viscosity ($Re \sim 10^7$), the descent rate intrinsic in the present domain size and vortex model appears to be $H/T = 0.98$, slightly less than ideal one.

To develop a model for vortex descent due to ambient turbulence, we first assume that the vortex descent rate is proportional to the circulation, that is,

$$\frac{\mathrm{d}h}{\mathrm{d}t} \sim \frac{\Gamma}{2\pi b_0} \tag{17}$$

or in the nondimensional form

$$\frac{\mathrm{d}H}{\mathrm{d}T} \sim \frac{\Gamma}{\Gamma_\infty} \tag{18}$$

For weak and moderate turbulence, the circulation is expected to decay as a Gaussian function, as discussed in the preceding section. Thus, substituting Eq. (14) into Eq. (18), we obtain

$$\frac{\mathrm{d}H}{\mathrm{d}T} \sim \exp\left[-(d_1 \eta T)^2\right] \tag{19}$$

where d_1 is an empirical coefficient. After integration, we finally obtain

$$H = (0.87/d_1\eta)\,\mathrm{erf}(d_1 \eta T) \tag{20}$$

where erf is an error function and the proportionality constant 0.87 is an optimal value determined from our LES results. The preceding model for vortex descent has been applied to our LES results for weak and moderate turbulence. As shown in Figs. 10a–10d,

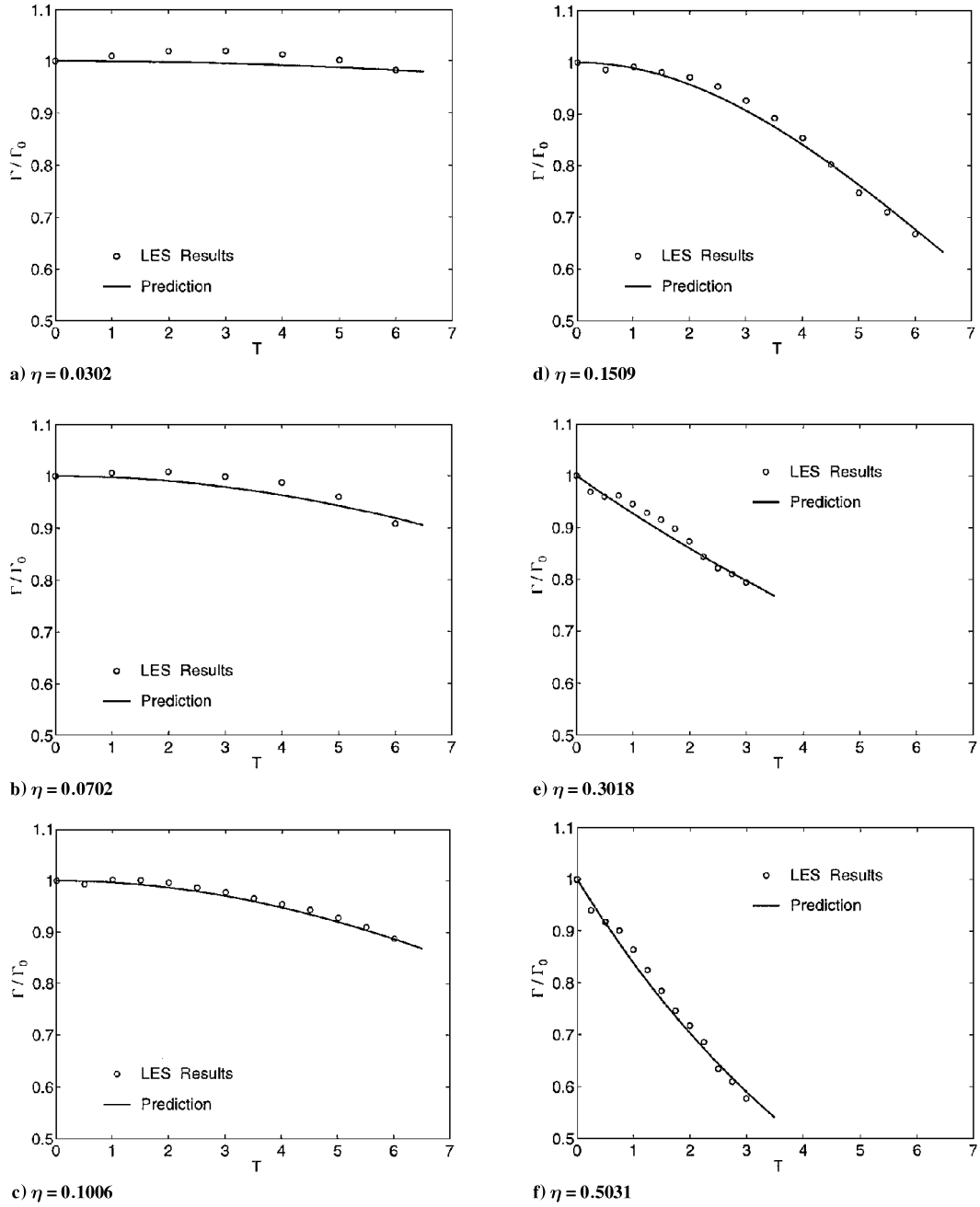

Fig. 7 Evolution of the circulation averaged from $R = 0.4$ to 0.6 and corresponding model prediction with the coefficient adjusted for a best fit.

the model predictions agree well with the LES data, although the best-fitted coefficient d_1 appears to fluctuate with varying η (Fig. 11).

For strong turbulence, however, an optimal value for d_1 could not be found. This may be because, for strong turbulence, the circulation decays exponentially over radial distances less than about $0.6b_0$, implying that circulations at smaller radial distances than $R = 0.6$ may also play significant role on the descent rate. Nevertheless, the modified form of Eq. (20)

$$H = (d_2/0.28\eta)\,\mathrm{erf}(0.28\eta T) \tag{21}$$

where d_2 is an empirical coefficient less than 0.87, can be matched with our LES results, as shown in Figs. 10e and 10f.

In the transition range from moderate to strong ambient turbulence levels, a simple model for $0.25 < \eta < 0.30$, similar to that for vortex decay, can be proposed:

$$H = [(\eta - \eta_1)/\Delta\eta]H_E + [(\eta_2 - \eta)/\Delta\eta]H_G \tag{22}$$

where H_E and H_G are the nondimensional vortex descent distance given by Eqs. (21) and (20), respectively.

The model coefficients d_1 and d_2 have been estimated the various LES cases covering a wide range of η values and are shown in Fig. 11. The variations around their mean values of $d_1 = 0.84$ and $d_2 = 0.71$ are less than 20%.

Using the given mean values of the coefficients, the model predictions for the vortex descent for various ambient turbulence levels are plotted in Fig. 12 with the vortex lifespans obtained from Sarpkaya's[9] model. Figure 12 shows clearly that the descent rate of the vortices decreases with increasing ambient turbulence due to the increasing rate of decay of circulation with increasing ambient turbulence. On the other hand, for weak turbulence, the descent distance appears to closely follow the line $H = 0.98T$ before the vortex linking occurs.

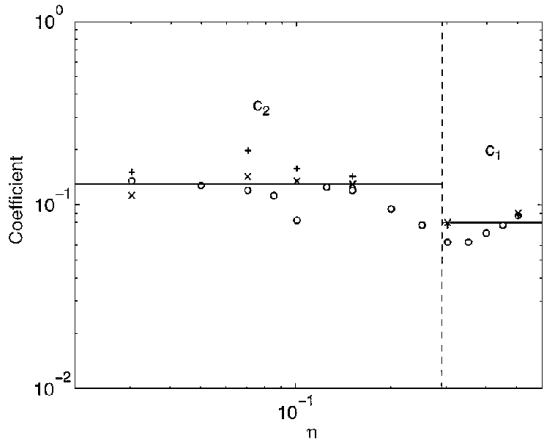

Fig. 8 Model coefficients with varying η for the circulation decay in Eqs. (13) and (14) as obtained from numerical simulations: same symbols represent the results from same initial turbulence fields; solid lines indicate the average values of the coefficients for the Gaussian and exponential models distinguished by dashed line.

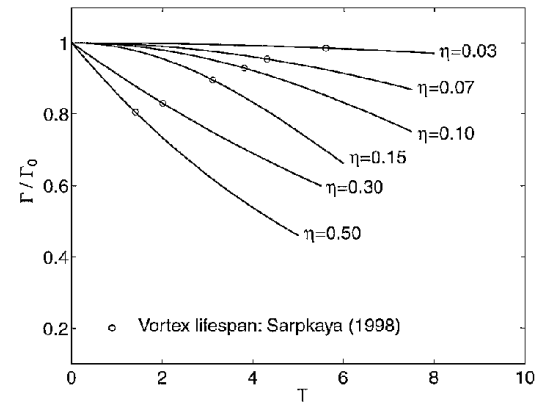

Fig. 9 Model prediction with varying η for the circulation at $R = 0.5$ with vortex lifespan presented.

IV. Comparison of Observation Data and Model Predictions

In this section predictions of wake vortex decay and descent from the models proposed in the preceding sections are compared to observation from the Memphis Field Program.[40] As part of the NASA sponsored field program, Massachusetts Institute of Technology Lincoln Laboratory operated 10.6 μm CO_2 continuous wave laser Doppler radar [light detection and ranging (LIDAR)] and measured the line-of-sight velocities of the vortices in a plane perpendicular to the flight path of approaching or departing aircraft. Circulation values were estimated from the measured line-of-sight velocity field.[40]

In this study, six cases (Table 2) are chosen based on atmospheric stability conditions and number of data points. Some of the cases have been also analyzed by Sarpkaya[9] for a different purpose. The proposed models only address the effect of ambient turbulence on vortex decay and do not include the effect of thermal stratification. The initial conditions for the proposed models used the representative vortex separation and far-field circulation in Table 2, as well as the TKE dissipation rate ϵ measured at 40 m (Table 3). As seen from Table 3, the η values calculated by the definition [Eq. (2)] are within the range of those used in our earlier LES.

Shown in Fig. 13 are the measured average circulations over the range of $R = 0.4-0.6$ with those from model predictions based on Eqs. (13) and (14) using the mean coefficients. The initial average circulation Γ_0 is determined from the present vortex model [Eq. (8)] with the theoretical circulation at $r \gg r_c$ (Γ_∞) given in Table 2. The

Table 2 Initial parameters for wake vortices for the flights analyzed

Flight number	Aircraft type	b_0, m	Γ_∞, $m^2\ s^{-1}$	Aircraft altitude, m	Atmospheric stability (observing time)
M-1252	B-757	29.8	323	160.2	Stable (midnight)
M-1273	DC-10	39.6	416	149.9	Stable (midnight)
M-1569	DC-9	22.4	241	127.5	Neutral (evening)
M-1573	DC-9	22.4	245	103.8	Neutral (evening)
M-1581	B-757	29.8	297	166.1	Unstable (noon)
M-1584	DC-9	22.4	231	125.7	Unstable (noon)

Table 3 Turbulence energy dissipation rate[a]

Flight number	ϵ, $m^2\ s^{-3}$	η
M-1252	0.212×10^{-5}	0.023
M-1273	0.150×10^{-6}	0.012
M-1569	0.584×10^{-3}	0.138
M-1573	0.255×10^{-3}	0.103
M-1581	0.302×10^{-2}	0.283
M-1584	0.366×10^{-2}	0.265

[a]Measured at elevation of 40 m and corresponding nondimensional turbulence intensity.

data for times less than $T = 1$ have been discarded from the data set for all of the cases analyzed because the observed circulations at these times are subject to large trigonometry errors, for example, see Ref. 40.

As seen in Fig. 13, predictions by the proposed models appear to underestimate considerably the observations except for the stronger turbulence cases of M-1581 and M-1584 in which the model predictions appear to be in reasonable agreement with observations. The underestimation also appears to be larger with decreasing η. Significant differences in the rate of decay for the weaker turbulence cases between model predictions and observations may be caused by the following possibilities: 1) For the stable cases of M-1252 and M-1273, the interaction between the vortices and stable stratification, which is not included in the present numerical simulations, may enhance vortex decay as discussed in the Introduction. 2) There may be additional turbulence not taken into account in our simulations, such as self-generated internal turbulence that may originate with the vortices during the initial rollup process and may be confined only within the vortex oval. (The internal turbulence may be more effective on vortex decay for weaker ambient turbulence.) 3) There is uncertainty in measurement data especially for initial circulation Γ_∞. (Note that the η value and the rate of vortex decay in the observations are quite sensitive to the initial circulation.) 4) There is a discrepancy in the computation of the circulation between the numerical simulations and observations. (The circulation in the simulations is obtained directly by integrating the axial vorticity field, whereas the measured circulation is estimated from LIDAR line-of-sight velocities.)

For possibility 1, the effect of the stable stratification on vortex decay can be easily incorperated into Eqs. (11) or (12). According to Greene,[8] the rate of circulation decay due to the stable stratification is given by

$$\left.\frac{d\Gamma}{dt}\right|_{\text{stratification}} = -\frac{AN^2h}{b_0} \tag{23}$$

where A is the wake oval area equal to $[\pi(1.73) \times (2.09)b_0^2]/4$. Because the ambient turbulence strength is generally weak in the stable atmosphere due to the suppression of ambient turbulence by stable stratification, for example see Table 2, Eq. (23) will be combined with model G [Eq. (12)] rather than model E [Eq. (11)] for a total vortex decay. Therefore, the total rate of circulation decay due to both ambient turbulence and stable stratification can be written in a nondimensional form as

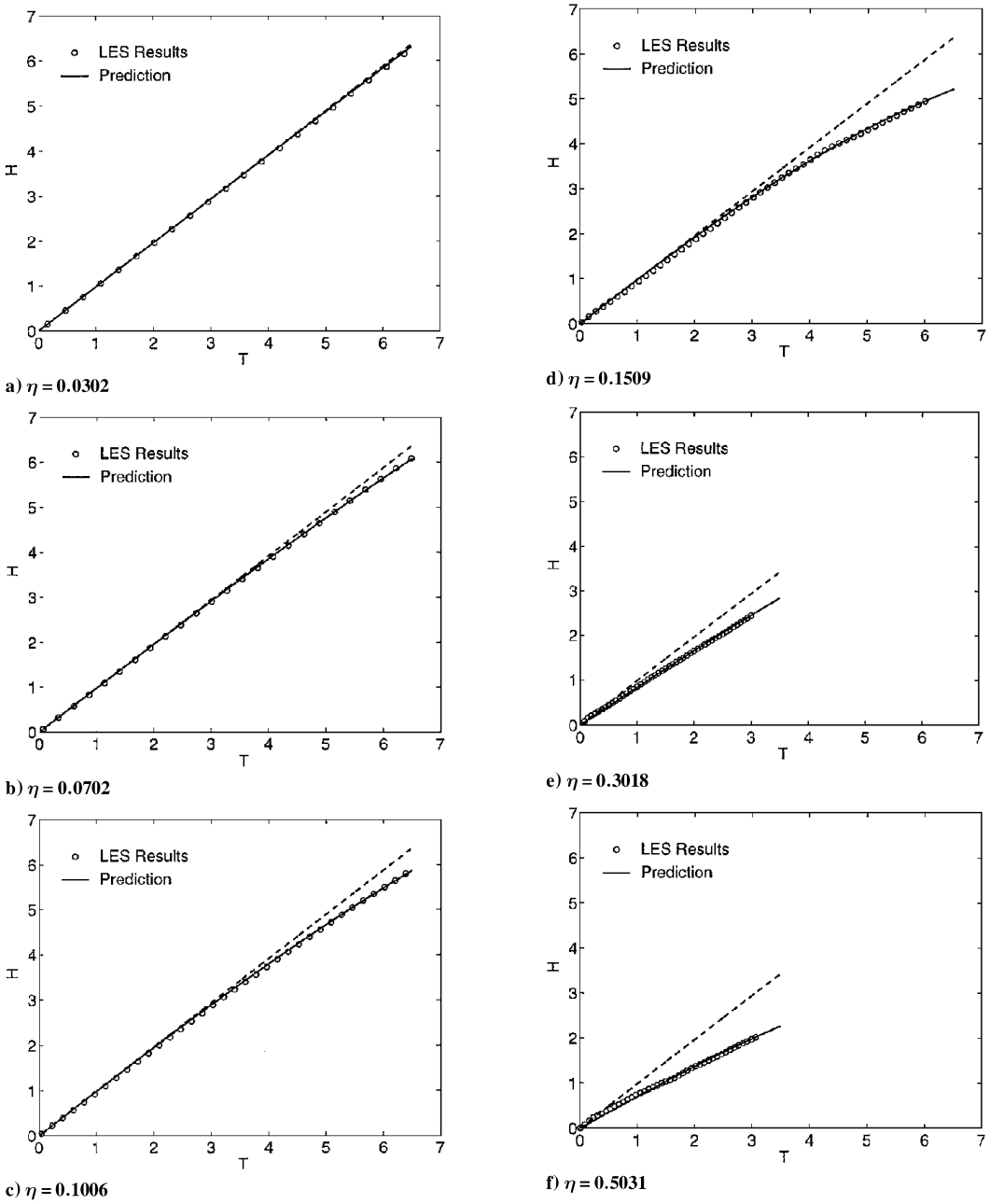

a) $\eta = 0.0302$

b) $\eta = 0.0702$

c) $\eta = 0.1006$

d) $\eta = 0.1509$

e) $\eta = 0.3018$

f) $\eta = 0.5031$

Fig. 10 Evolution of the descent distance in three-dimensional simulations compared with the theoretical model: dashed line $H = 0.98T$.

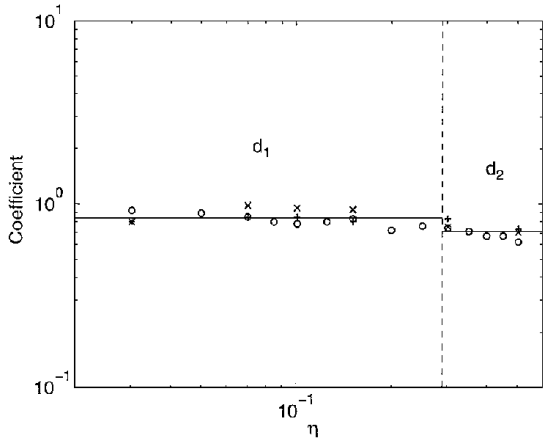

Fig. 11 Same as Fig. 8 but for the vortex descent in Eqs. (20) and (21).

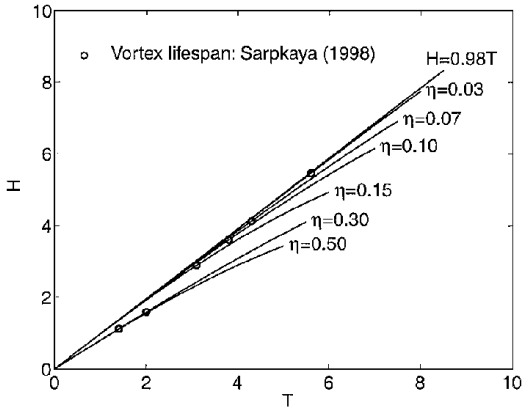

Fig. 12 Same as in Fig. 9 but for the vortex descent.

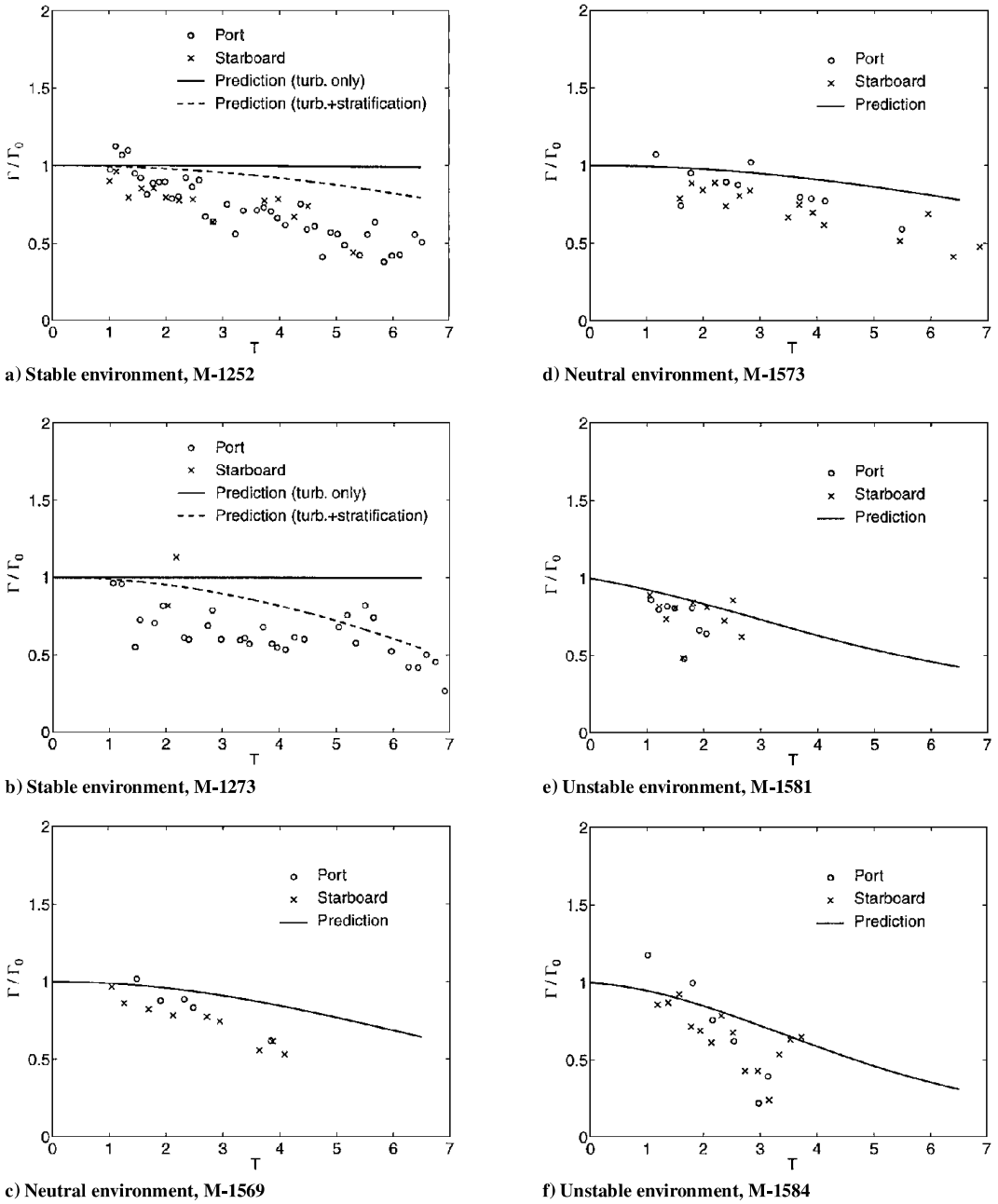

a) Stable environment, M-1252

d) Neutral environment, M-1573

b) Stable environment, M-1273

e) Unstable environment, M-1581

c) Neutral environment, M-1569

f) Unstable environment, M-1584

Fig. 13 Comparison of field observations and model predictions for the average circulation over the range $R = 0.4-0.6$; solid (dashed) lines are model predictions for the circulation decay due to ambient turbulence only (due to both ambient turbulence and stable stratification).

$$\left.\frac{d\Gamma}{dT}\right|_{\text{turbulence}} = \left.\frac{d\Gamma}{dT}\right|_{\text{turbulence}} + \left.\frac{d\Gamma}{dt}\right|_{\text{stratification}}$$

$$= -2c_2\frac{\eta^2 T}{R^2}\Gamma - \frac{b_0 A N^2 H}{V_0} \tag{24}$$

On the other hand, the rate of vortex descent is given by

$$\frac{dH}{dT} = \frac{\Gamma}{\Gamma_0} \tag{25}$$

Vortex decay and descent in Eqs. (24) and (25) have been computed through a numerical integration using a forward scheme in time, based on a vertically averaged N from the observed ambient potential temperature profile [N^2 is defined as $(g/\Theta)(\partial\Theta/\partial z)$, where g is the gravitational acceleration]. As shown in Figs. 13a and 13b, when the stratification effect is added in the model, the underestimation in vortex decay is significantly reduced, indicating that stratification has an important influence on vortex decay for a weak ambient turbulence with stable stratification.

Shown in Fig. 14 are the measured vortex descents with model predictions based on Eqs. (20) and (21) again using the mean coefficients. In the calculation, the starting altitude of the vortices has been inferred from the LIDAR measurement as by Robins et al.[41] because the vortices appears to be located above the expected position, that is, the generating aircraft height in Table 2. Consistent with the large underestimation for the circulation decay, the model predictions in the weaker turbulence cases of M-1252 and M-1273 with stable stratification significantly overestimate the observed vortex descent, especially at later time periods. However, this overestimation in vortex descent is significantly reduced when the stratification effect is added in the model, consistent with reduction of the underestimation in circulation decay. The model predictions for the stronger turbulence cases of M-1581 and M-1584 appear to be in reasonable agreement with observations, which is also consistent with the agreement for the circulation decay.

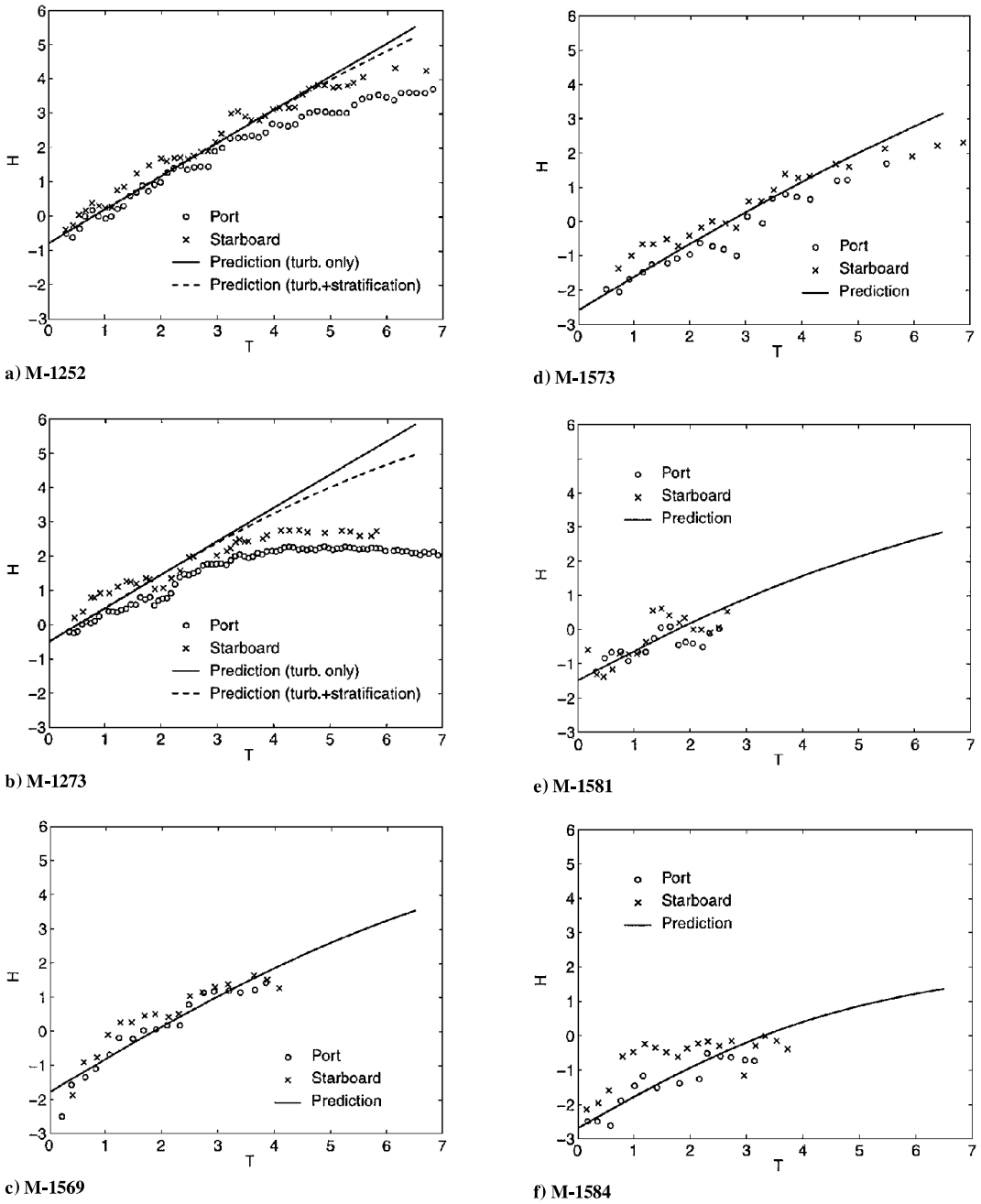

Fig. 14 Same as Fig. 13 but for the vortex descent.

V. Conclusions

This study represents a first step at understanding how wake vortices behave in the atmosphere by isolating the effects of ambient turbulence on vortex decay. LES simulations are conducted by first inducing a field of ambient turbulence that is nearly isotropic and spatially homogeneous. A vortex pair, representing aircraft trailing vortices, is introduced once the turbulence field reaches a statistically steady state. In these simulations, the Crow linking and its subsequent effect on vortex decay are suppressed by the selection of axial domain size.

Our results show that, consistent with field observations, the decay rate of the vortex circulation increases clearly with increasing levels of ambient turbulence and decreases with increasing radial distance. Based on the LES results, simple decay models for the vortex pair are proposed as functions of nondimensional ambient turbulence intensity η, nondimensional radial distance R, and nondimensional time T. Showing good agreement with the LES data, we propose a Gaussian type of vortex decay model for weak and moderate turbulence, whereas an exponential type of vortex decay model is more appropriate for strong turbulence. The LES simulations and the fitted models show that the turbulence dissipation rate characterizes the level of ambient turbulence responsible for vortex decay. A model for the vortex descent based on the given vortex decay model is also proposed with functions of η and T and can be represented by an error function.

The proposed models for the vortex decay and descent are applied to available field data obtained from the Memphis airport. For a strong atmospheric turbulence, the model predictions appear to be in reasonable agreement with the observation data. For a weak atmospheric turbulence with stable stratification, the models largely underestimate the observed circulation decay with consistent overestimation of the observed vortex descent. However, this underestimation in vortex decay is significantly reduced with consistent reduction of the overestimation in vortex descent when the stratification effect is added in the models, indicating that stratification has an important influence on vortices for weak ambient levels of

turbulence under stably stratified conditions. The lack of agreement in the rate of decay for the weaker turbulence cases between model predictions and observations may also be caused by some other factors that are not taken into account in the comparison, such as the effect of internal turbulence on vortex decay, uncertainty in measurement data, and discrepancy in computation of the circulation between numerical simulations and observations.

Appendix: Derivation of Decay Models

For high-Reynolds-number flows under the condition of neutral stratification, the equation that governs the rate of change for mean axial vorticity $\bar{\zeta}$ due to turbulent motion can be given by

$$\frac{d\bar{\zeta}}{dt} = -\frac{\partial}{\partial x_j}\overline{u_j'\zeta'} \tag{A1}$$

Integration of Eq. (A1) over the region defined by the radial distance r yields

$$\iint \frac{d\bar{\zeta}}{dt}\,dA = -\iint \frac{\partial}{\partial x_j}\overline{u_j'\zeta'}\,dA \tag{A2}$$

The area integral on the right-hand side of Eq. (A2) can be transformed into a line integral taken around the perimeter of the area using the Stoke's theorem, that is,

$$\frac{d\Gamma}{dt} = -\oint \overline{u_n'\zeta'}\,ds \tag{A3}$$

where u_n' is the fluctuation of velocity normal to the surface. The line integral leads to

$$\frac{d\Gamma}{dt} = -2\pi r\langle\overline{u_n'\zeta'}\rangle \tag{A4}$$

where $\langle\ \rangle$ denotes an average around the perimeter with the radial distance r. From the down-gradient transport approximation,

$$\langle\overline{u_n'\zeta'}\rangle \sim -\nu_e\frac{\partial\langle\bar{\zeta}\rangle}{\partial r} \tag{A5}$$

where ν_e is an effective eddy viscosity. The radial gradient of mean axial vorticity may be approximated by

$$\frac{\partial\langle\bar{\zeta}\rangle}{\partial r} \sim -\frac{\langle\bar{\zeta}\rangle}{r} \tag{A6}$$

$$\langle\bar{\zeta}\rangle \sim \frac{\Gamma}{r^2} \tag{A7}$$

so that

$$\frac{\partial\langle\bar{\zeta}\rangle}{\partial r} \sim -\frac{\Gamma}{r^3} \tag{A8}$$

Note that $\partial\langle\bar{\zeta}\rangle/\partial r$ is assumed to be proportional to the difference of mean axial vorticity at the vortex center and that at the radial distance r. We are basically considering a vortex flow in which deviation from the axisymmetry due to ambient turbulence is small enough for the approximations of Eqs. (A5–A8) to be valid. Then Eq. (A4) can be expressed as

$$\frac{d\Gamma}{dt} \sim -\frac{\nu_e\Gamma}{r^2} \tag{A9}$$

The preceding derivations are almost the same as Donaldson and Bilanin's[7] (DB) except that the dependency of the circulation decay on the radial distance r is considered in the present study, whereas b_0 is used instead of r in DB's study because DB consider the decay rate of the circulation over an oval within which a pair of vortices resides.

From an equilibrium second-order closure theory, DB obtain the relation

$$\nu_e = 0.26\Lambda q \tag{A10}$$

where Λ is a measure of the integral length scale of turbulence. Assuming that

$$\Lambda \simeq b_0/8 \tag{A11}$$

DB then obtain Eq. (1). However, their approximation of Eq. (A11) is not physically correct because b_0 has no relation with background atmospheric turbulence whose length scale varies significantly over day and night. As discussed in the Introduction, we use ϵ, rather than q and Λ, as the ambient turbulence parameter relevant to circulation decay.

For strong turbulence but at smaller radial distances where stronger the radial gradient of mean axial vorticity may exist, the parameterization of Eq. (A5) would be acceptable. The effective eddy viscosity in this case can be expressed in terms of effective turbulence velocity and length scales, that is,

$$\nu_e \sim (\epsilon b_0)^{\frac{1}{3}} b_0 \tag{A12}$$

Note that $(\epsilon b_0)^{1/3}$ is a characteristic turbulence velocity scale at the scale of the vortex separation distance b_0. Substituting Eq. (A12) into Eq. (A9), we obtain

$$\frac{d\Gamma}{dt} \sim -\frac{(\epsilon b_0)^{\frac{1}{3}} b_0}{r^2}\Gamma \tag{A13}$$

Thus, the decay rate of the circulation depends on both the turbulence energy dissipation rate ϵ and radial distance r, unlike DB's model [Eq. (1)].

For weak and moderate turbulence or at larger radial distances for strong turbulence where the radial gradient of mean axial vorticity may be weak, the parameterization of Eq. (A5) would not be appropriate. It is anticipated that the radial turbulent vorticity flux $\overline{u_n'\zeta'}$ in this case will be mostly influenced by turbulent diffusion of vorticity from the core region rather than by local diffusion as in Eq. (A5). This implies that $\overline{u_n'\zeta'}$ would be time dependent. We then hypothesize that the rate of change of $\langle\overline{u_n'\zeta'}\rangle$ in this case depends on turbulence velocity and mean axial vorticity gradient from vortex center to given r, that is,

$$\frac{\partial\langle\overline{u_n'\zeta'}\rangle}{\partial t} = f\left((\epsilon b_0)^{\frac{1}{3}}, \frac{\Gamma}{r^3}\right) \tag{A14}$$

From dimensional arguments,

$$\frac{\partial\langle\overline{u_n'\zeta'}\rangle}{\partial t} \sim \frac{(\epsilon b_0)^{\frac{2}{3}}\Gamma}{r^3} \tag{A15}$$

Integration of Eq. (A15) with respect to time leads to

$$\langle\overline{u_n'\zeta'}\rangle \sim \left[(\epsilon b_0)^{\frac{2}{3}} t\Gamma \middle|\ r^3\right] \tag{A16}$$

where the initial value of $\langle\overline{u_n'\zeta'}\rangle$ is assumed to be zero. Substituting Eq. (A16) into Eq. (A4), we obtain

$$\frac{d\Gamma}{dt} \sim -\frac{(\epsilon b_0)^{\frac{2}{3}} t}{r^2}\Gamma \tag{A17}$$

Acknowledgments

This work was supported by NASA's Terminal Area Productivity Program under Contract NAS 1-18925 (Cooperative Agreement NCC-1-188). Numerical simulations were carried out on NASA's Cray C90 and J90 and North Carolina Supercomputing Center's Cray T916.

References

[1]Hinton, D. A., "Aircraft Vortex Spacing System (AVOSS) Conceptual Design," NASA TM-110184, Aug. 1995.

[2]Perry, R. B., Hinton, D. A., and Stuever, R. A., "NASA Wake Vortex Research for Aircraft Spacing," AIAA Paper 97-0057, Jan. 1997.

[3]Proctor, F. H., "The NASA-Langley Wake Vortex Modeling Effort in Support of an Operational Aircraft Spacing System," AIAA Paper 98-0589, Jan. 1998.

[4]Spalart, P. R., "Wake Vortex Physics: The Great Controversies," *NASA First Wake Vortex Dynamic Spacing Workshop*, NASA CP-97-206235, 1997, pp. 33, 34.

[5]Crow, S. C., "Stability Theory for a Pair of Trailing Vortices," *AIAA Journal*, Vol. 8, No. 12, 1970, pp. 2172–2179.

[6]Spalart, P. R., "Airplane Trailing Vortices," *Annual Review of Fluid Mechanics*, Vol. 30, 1998, pp. 1–35.

[7]Donaldson, C. duP., and Bilanin, A. J., "Vortex Wakes of Conventional Aircraft," AGARDograph 204, May 1975.

[8]Greene, G. C., "An Approximate Model of Vortex Decay in the Atmosphere," *Journal of Aircraft*, Vol. 23, No. 7, 1986, pp. 566–573.

[9]Sarpkaya, T., "Decay of Wake Vortices of Large Aircraft," *AIAA Journal*, Vol. 36, No. 9, 1998, pp. 1671–1679.

[10]Bilanin, A. J., Teske, M. E., and Hirsch, J. E., "Neutral Atmospheric Effects on the Dissipation of Aircraft Vortex Wakes," *AIAA Journal*, Vol. 16, No. 9, 1978, pp. 956–961.

[11]Corjon, A., and Darracq, D., "Three-Dimensional Large Eddy Simulation of Wake Vortices. Comparison with Field Measurements," AIAA Paper 97-2309, June 1997.

[12]Han, J., Lin, Y.-L., Schowalter, D. G., Arya, S. P., and Proctor, F. H., "Large-Eddy Simulation of Aircraft Wake Vortices: Atmospheric Turbulence Effects," *12th Symposium on Boundary Layers and Turbulence*, American Meteorological Society, Boston, 1997, pp. 237, 238.

[13]Han, J., Lin, Y.-L., Arya, S. P., and Kao, C., "Large-Eddy Simulation of Aircraft Wake Vortices: Atmospheric Turbulence Effects," *NASA First Wake Vortex Dynamic Spacing Workshop*, NASA CP-97-206235, 1997, pp. 131–144.

[14]Sarpkaya, T., and Daly, J. J., "Effect of Ambient Turbulence on Trailing Vortices," *Journal of Aircraft*, Vol. 24, No. 6, 1987, pp. 399–404.

[15]Sarpkaya, T., "Trailing Vortices in Homogeneous and Density-Stratified Media," *Journal of Fluid Mechanics*, Vol. 136, 1983, pp. 85–109.

[16]Hallock, J. N., and Burnham, D. C., "Decay Characteristics of Wake Vortices from Jet Transport Aircraft," AIAA Paper 97-0060, Jan. 1997.

[17]Tombach, I., "Observations of Atmospheric Effects on Vortex Wake Behavior," *Journal of Aircraft*, Vol. 10, No. 11, 1973, pp. 641–647.

[18]Spalart, P. R., and Wray, A. A., "Initiation of the Crow Instability by Atmospheric Turbulence," *78th AGARD-FDP Symposium on the Characterization and Modification of Wakes from Lifting Vehicles in Fluids*, 1996.

[19]Han, J., Lin, Y.-L., Schowalter, D. G., Arya, S. P., and Proctor, F. H., "Large Eddy Simulation of Aircraft Wake Vortices Within Homogeneous Turbulence: Crow Instability," *AIAA Journal*, Vol. 38, No. 2, 2000, pp. 292–300.

[20]Kolmogorov, A. N., "The Local Structure of Turbulence in Incompressible Viscous Fluid for Very Large Reynolds Number," *Doklady Akademii Nauk SSSR*, Vol. 30, 1941, pp. 9–13.

[21]Crow, S. C., and Bate, E. R., "Lifespan of Trailing Vortices on a Turbulent Atmosphere," *Journal of Aircraft*, Vol. 13, No. 7, 1976, pp. 476–482.

[22]Liu, H.-T., "Effects of Ambient Turbulence on the Decay of a Trailing Vortex Wake," *Journal of Aircraft*, Vol. 29, No. 2, 1992, pp. 255–263.

[23]Proctor, F. H., "The Terminal Area Simulations System, Volume 1: Theoretical Formulation," NASA CR 4046, Dept. of Transportation/Federal Aviation Administration/PM-86/50, 1, 1987.

[24]Proctor, F. H., "Numerical Simulation of Wake Vortices Measured During the Idaho Fall and Memphis Field Programs," *Proceedings of the AIAA 14th Applied Aerodynamics Conference*, Pt. 2, AIAA, Reston, VA, 1996, pp. 943–960.

[25]Proctor, F. H., Hinton, D. A., Han, J., Schowalter, D. G., and Lin, Y.-L., "Two-Dimensional Wake Vortex Simulations in the Atmosphere: Preliminary Sensitivity Studies," AIAA Paper 97-0056, Jan. 1997.

[26]Schowalter, D. G., Decroix, D. S., Switzer, G. F., Lin, Y.-L., and Arya, S. P., "Toward Three-Dimensional Modeling of a Wake Vortex Pair in the Turbulent Boundary Layer," AIAA Paper 97-0058, Jan. 1997.

[27]Klemp, J. B., and Wilhelmson, R. B., "The Simulation of Three-Dimensional Convective Storm Dynamics," *Journal of Atmospheric Sciences*, Vol. 35, No. 6, 1978, pp. 1070–1096.

[28]Switzer, G. F., "Validation Tests of TASS for Application to 3-D Vortex Simulation," NASA CR 4756, 1996.

[29]Lord Rayleigh, "On the Dynamics of Revolving Fluids," *Proceedings of the Royal Society of London Series A: Mathematical and Physical Sciences*, Vol. 93, 1916, p. 148.

[30]Smagorinsky, J., "General Circulation Experiments with the Primitive Equations: I. The Basic Experiments," *Monthly Weather Review*, Vol. 91, No. 3, 1963, pp. 99–164.

[31]Proctor, F. H., "A LES Subgrid Turbulence Model with Rotational Dampening," NASA TR, 1999.

[32]Rubinstein, R., and Zhou, Y., "The Dissipation Rate Transport Equation and Subgrid-Scale Models in Rotating Turbulence," NASA CR-97-206250, Inst. for Computer Applications in Science and Engineering, Rept. 97-63, Nov. 1997.

[33]Han, J., "Large Eddy Simulations of Aircraft Wake Vortices in a Homogeneous Atmospheric Turbulence," Ph.D. Dissertation, North Carolina State Univ., Raleigh, NC, 1998.

[34]Vincent, A., and Meneguzzi, M., "The Spatial Structure and Statistical Properties of Homogeneous Turbulence," *Journal of Fluid Mechanics*, Vol. 225, 1991, pp. 1–20.

[35]Lamb, H., *Hydrodynamics*, 6th ed., Cambridge Univ. Press, New York, 1932.

[36]Corjon, A., Risso, F., Stoessel, A., and Poinsot, T., "Three-Dimensional Direct Numerical Simulations of Wake Vortices: Atmospheric Turbulence Effects and Rebound with Crosswind," *78th AGARD–FDP Symposium on the Characterization and Modification of Wakes from Lifting Vehicles in Fluids*, 1996, pp. 28-1–28-21.

[37]Burnham, D. C., and Hallock, J. N., "Chicago Monostatic Acoustic Vortex Sensing System," Dept. of Transportation–TSC–Federal Aviation Administration Rept. DOT-TSC-FAA-79-103 IV, July 1982; available from National Technical Information Service.

[38]Hinton, D. A., and Tatnall, C. R., "A Candidate Wake Vortex Strength Definition for Application to the NASA Aircraft Vortex Spacing System (AVOSS)," NASA TM-110343, Sept. 1997.

[39]Tatnall, C. R., "An Investigation of Candidate Sensor-Observable Wake Vortex Strength Parameters for the NASA Aircraft Vortex Spacing System (AVOSS)," NASA CR-1998-206933, March 1998.

[40]Campbell, S. D., Dasey, T. J., Freehart, R. E., Heinrichs, R. M., Matthews, M. P., Perras, G. H., and Rowe, G. S., "Wake Vortex Field Measurement Program at Memphis, TN Data Guide," Project Report: NASA/L-2, Jan. 1997; available from National Technical Information Service.

[41]Robins, R. E., Delisi, D. P., and Greene, G. C., "Development and Validation of a Wake Vortex Predictor Algorithm," AIAA Paper 98-0665, Jan. 1998.

J. R. Bellan
Associate Editor